ground water

Evaluating MT3DMS for Heat Transport Simulation of Closed Geothermal Systems

by Jozsef Hecht-Méndez[1], Nelson Molina-Giraldo[2], Philipp Blum[2], and Peter Bayer[3]

Abstract

Owing to the mathematical similarities between heat and mass transport, the multi-species transport model MT3DMS should be able to simulate heat transport if the effects of buoyancy and changes in viscosity are small. Although in several studies solute models have been successfully applied to simulate heat transport, these studies failed to provide any rigorous test of this approach. In the current study, we carefully evaluate simulations of a single borehole ground source heat pump (GSHP) system in three scenarios: a pure conduction situation, an intermediate case, and a convection-dominated case. Two evaluation approaches are employed: first, MT3DMS heat transport results are compared with analytical solutions. Second, simulations by MT3DMS, which is finite difference, are compared with those by the finite element code FEFLOW and the finite difference code SEAWAT. Both FEFLOW and SEAWAT are designed to simulate heat flow. For each comparison, the computed results are examined based on residual errors. MT3DMS and the analytical solutions compare satisfactorily. MT3DMS and SEAWAT results show very good agreement for all cases. MT3DMS and FEFLOW two-dimensional (2D) and three-dimensional (3D) results show good to very good agreement, except that in 3D there is somewhat deteriorated agreement close to the heat source where the difference in numerical methods is thought to influence the solution. The results suggest that MT3DMS can be successfully applied to simulate GSHP systems, and likely other systems with similar temperature ranges and gradients in saturated porous media.

Introduction

MT3DMS (Zheng and Wang 1999) is a widely used program for simulation of solute transport in porous media. Since the governing equations for solute transport are mathematically identical to those for heat transport, this program appears also applicable to simulation of thermal transport phenomena in saturated aquifers. This is demonstrated in recent case studies. Martin et al. (2001) used MT3DMS to simulate heat transport on Grand Cayman Island. Cathomen (2002) and Cathomen et al. (2002) applied MT3DMS to assess the groundwater temperature distribution in an urban area of the Altach Municipality (Austria) under the influence of several ground source heat pump (GSHP) systems.

Using MT3DMS for heat transport in aquifers has limitations, because it is decoupled from the flow model. MT3DMS uses the flow regime predicted by flow simulators such as MODFLOW (Harbaugh et al. 2000) without feedback. However, in principle this is necessary, because temperature variation affects water viscosity and density, which effect hydraulic conductivity. Temperature variations in the shallow subsurface commonly are small, so simulation errors produced from using constant viscosity and density often are small and acceptable. Shallow geothermal systems produce conditions for which

[1]Corresponding author: Center for Applied Geoscience (ZAG), University of Tübingen, Sigwartstrasse 10, 72076 Tübingen, German; +49-7071-2973172; fax: +49-7071-295059; jozsef.hecht-mendez@uni-tuebingen.de

[2]Center for Applied Geoscience (ZAG), University of Tübingen, Sigwartstrasse 10, 72076 Tübingen, Germany.

[3]ETH Zürich, Ecological System Design, Institute for Environmental Engineering, Schafmattstrasse 6, 8093 Zurich, Switzerland, now at Geological Institute, ETH Zurich, Sonneggstrasse 5, CH-8092 Zurich, Switzerland.

Received April 2009, accepted December 2009.

doi: 10.1111/j.1745-6584.2010.00678.x

such errors are likely to be inconsequential. Evaluating the utility of MT3DMS for shallow geothermal systems is the topic of the presented study.

Geothermal energy is the form of energy stored as heat in the soil, rocks, and fluids below the surface of the solid earth. It is available almost everywhere and it represents an enormous source of energy which can be applied in, for example, electricity generation, process heating, and space heating (e.g., Clauser 2006). Geothermal energy usage has shown a continuous and rapid development within the last decades. Considering the trends in global annual energy production of the different applications (Bertani 2005; Lund et al. 2005), for the period from 2000 to 2005, an annual growth rate of 10% can be estimated. The use of this energy has become attractive due to inherent savings of fossil fuels and relatively low CO_2 emissions. Blum et al. (2010) provide values for CO_2 savings when using GSHP systems for heating or cooling of buildings. For instance, by using a GSHP system for heating a single family house in Central Europe, at least 35% of additional CO_2 emissions can be avoided in comparison to conventional heating systems.

Geothermal systems for heating/cooling of building and facilities use heat available in the upper part of the subsurface (down to 400 m). This is often done via GSHP systems, which are installed underground, usually down to depths of 150 m. Two types of shallow geothermal systems can be generally distinguished, closed, and open systems (Figure 1); the latter is defined as a groundwater heat pump (GWHP) system. In the current study, closed shallow geothermal systems are considered and are referred to as GSHP. Closed systems employ one or more pipes or borehole heat exchangers (BHEs). The heat stored in the ground is mined through a segregate heat carrier fluid inside the BHE and extracted by a heat pump on the surface. In contrast, open systems operate with groundwater production and injection wells; groundwater at a certain temperature is directly brought to the surface. A comprehensive review of these systems is provided by Florides and Kalogirou (2007).

Depending on the use mode (heating or cooling), energy can be extracted or injected. Thus, the ambient aquifer temperature is disturbed and cold or warm plumes develop. These disturbances are compensated by lateral conductive heat transport and by convection due to moving water. The efficiency of geothermal technologies depends on the prevalent hydrogeological and thermal conditions. Proper installation and efficient maintenance requires an appropriate characterization of the heat transport processes, conduction, and convection, in the subsurface.

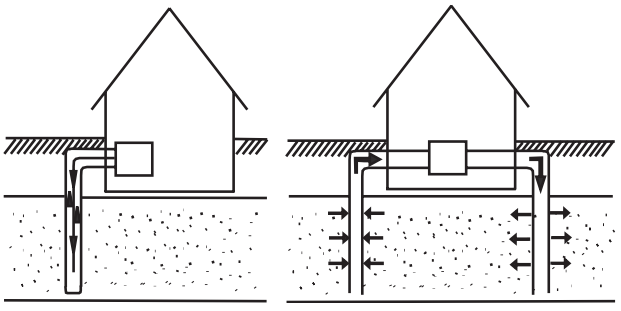

Figure 1. Scheme of shallow geothermal systems that are closed (left, GSHP system) and open (right, GWHP system).

Among others, Eskilson (1987), Chiasson et al. (2000), Diao et al. (2004), Fan et al. (2007), and Guimera et al. (2007) simulated the effects of groundwater flow on the heat transfer into the BHEs in vertical closed systems. A common conclusion is that, for material with high hydraulic conductivity and thus high discharge rates, groundwater flow enhances heat transfer between BHEs and the surrounding aquifer. Therefore, it is essential to have tools that allow for the evaluation not only of technical aspects of GSHP systems but also the effects of groundwater flow on the system efficiency and, further, the temperature changes in the aquifer exerted by the energy extraction or injection rates. Indeed, as recently mentioned by Ferguson (2009), this last aspect is closely related to the environmental impact and sustainability of such systems, and to the temperature propagation of one or several GSHP systems.

Numerical heat transport models are widely used, such as for design of BHEs, regional heat transport modeling, seasonal aquifer thermal energy storage (ATES), and technico-economic system design (Tsang et al. 1981; Chiasson et al. 2000; Hellström and Schmidt 2005). The development of numerical codes for heat and solute transport has been closely related to the advent of more powerful computers. In an early stage of numerical simulation, only simple one-dimensional (1D) problems were conducted while, today, more complicated problems with complex boundary conditions can be efficiently handled (Anderson 2005). Heat simulation codes allow for simulating one-, two-, and three-dimensional problems. Table 1 offers a comprehensive list of models that have been used or are potentially suitable for both convective and conductive heat transport simulations of shallow GSHP systems. Anderson (2005) provided a similar table; Table 1 lists some additional codes not considered by Anderson (2005), but is still not considered to be exhaustive.

In these models, the coupling of the groundwater flow simulation and the heat transport calculation is done by means of Darcy's velocity. Codes such as: AST/TWOW, TRADIKON3D, and VS2DH feature one-way coupling between flow and transport, that is, the flow field is calculated once at the beginning of the overall simulation and then used as an input for the transport simulation without there being any feedback to the flow simulation. The remaining codes can be classified as fully coupled and can handle temperature dependencies of density and viscosity. Some codes (e.g., FEFLOW, FRACHEM, and SHEMAT) couple hydraulic, thermal, and chemical processes. Such processes are common in deep environments with high temperatures; therefore, these codes are also suitable for deep geothermal assessment (e.g., Hot Dry Rock, HDR). Others have specialized routines which allow for simulation of mechanical deformation processes (BASIN2,

Table 1
Numerical Codes Suitable for Heat Transport Simulations of Shallow Geothermal Systems Considering Groundwater Flow (Not Meant to Be Exhaustive or Complete)

Code Name	Numerical Method	Processes	Coupling of Processes[1]	Availability	Comments	References
AST/TWOW[2]	FD	H, T	H → T	Commercial	3D, calculates near-field heat transport around BHEs	Schmidt and Hellström (2005)
BASIN2	FD	H, T, C	H ↔ T, M, CH	Free code	2D, simulates sedimentary basin development. Cross-sectional view	Bethke et al. (2007)
COMSOL[2]	FE	H, T, C	H ↔ T	Commercial	3D, multi-physics (more processes can be coupled)	Holzbecher and Kohfahl (2008)
FEFLOW[2]	FE	H, T , C	H ↔ T, M, C	Commercial	2D, 3D	Diersch (2002)
FRACHEM	FE	H, T, C	H ↔ T, M, C	Scientific	3D, used for Hot Dry Rock modeling	Bächler (2003)
FRACture[2]	FE	H, T	H ↔ T, M	Scientific	3D, developed for Hot Dry Rock modeling	Kohl and Hopkirk (1995)
ROCKFLOW/GeoSys	FE	H, T , C	H ↔ T, C	Scientific	3D, fracture systems can be included. Allows for multi-phase flow	Kolditz et al. (2001)
HEATFLOW[2]	FE	H, T	H ↔ T	Free code	1D, 2D, 3D	Molson and Frind (2002)
HST2D/3D	FD	H, T, C	H ↔ T, M, CH	Free code	2D, 3D	Kipp (1986)
HydroTherm	FD	H, T	H ↔ T	Free code	2D, 3D, two-phase model. Can simulate 0 to 1200 °C	Kipp et al. (2008)
HYDRUS-2D	FE	H, T, C	H → T	Commercial	2D, unsaturated zone, plant water uptake is considered	Šimùnek et al. (1999)
SEAWAT	FD	H, T, C	H ↔ T, C	Free code	3D	Langevin et al. (2008)
SHEMAT[2]	FD	H, T, C	H ↔ T, C	Commercial	3D	Clauser (2003)
SUTRA	FE/FD	H, T, C	H ↔ T, C	Free code	2D, 3D	Voss and Provost (2002)
THETA[2]	FD	H, T, C	H ↔ T, CH	Scientific	3D	Kangas (1996)
TOUGH2	FD	H, T, C	H ↔ T, C, CH	Commercial	1D, 2D, and 3D, one of the most widely used code in geothermal energy technologies. Allows for multi-phase flow	Pruess et al. (1996)
TRADIKON 3D[2]	FD	H, T	H → T	Free code	3D, specially designed for BHEs assessments	Brehm (1989)
VS2DH	FD	H, T	H → T	Free code	2D	Healy and Ronan (1996)

Note: H, Hydraulic; T, Temperature; C, Contaminant (solute).
[1]H → T, fluid flow is independent of T; H ↔ T, fluid flow depends on T; M, mechanical deformation (pore deformation); CH, chemical reaction.
[2]Already used for GSHP simulations.

FRACHEM, FRACture, ROCKFLOW/GeoSys). Some routines were originally developed for assessing shallow geothermal systems, such as GSHPs or energy storage systems (e.g., HEATFLOW, THETA), and others specifically for GSHP simulations (e.g., AST/TWOW, TRADIKON 3D). In addition to these numerical codes, there are other advanced routines such as HydroGeoSphere (finite elements, Therrien et al. 2006) and ParFlowE (finite differences, Kollet et al. 2009), which both allow for fully coupled simulations of surface flow, subsurface flow, and energy transport processes.

Aside from MT3DMS, other solute transport codes have also been used for heat transport simulations. For example, Chiasson et al. (2000) evaluated the effect of groundwater flow on a BHE using AQUAD3D, software developed for contaminant transport. Guimera et al. (2007) used the solute transport model TRANSIN (Medina et al. 1996) to simulate heat transport of open systems near Barcelona, Spain. In their work, the thermal impact of several production wells on groundwater is predicted. Thorne et al. (2006) added heat transport (including temperature dependency of the fluid density and viscosity) to the USGS density variable fluid code SEAWAT (Langevin et al. 2003) and solved the classic Henry-Hilleke problem, which involves a salt water intrusion in coastal areas. SEAWAT is based on the well-known codes MODFLOW and MT3DMS. In their approach, heat is introduced as a single contaminant species.

Although in several studies solute transport models were successfully applied for simulating heat transport, a rigorous test of this transfer is missing, and consequently simulations of GSHP systems with such codes do not have a credible background. The presented study provides a comprehensive evaluation of MT3DMS version 5.2 for its application in two-dimensional (2D) and three-dimensional (3D) heat transport simulations of closed GSHP systems. These systems are considered for various generic scenarios that are distinguished by the Péclet number. Two types of tests are employed. First, numerical results are compared with standard solute and heat transport analytical solutions. For 2D scenarios, line-source analytical solutions for heat transport simulation are applied (Carslaw and Jäger 1959; Diao et al. 2004; Metzger et al. 2004). For 3D scenarios, planar-source analytical solutions based on classical solute transport equations are considered (Fried et al. 1979; Domenico and Robbins 1985; Hähnlein et al. in press). Note that the selected analytical solutions do not consider temperature dependency of groundwater density and viscosity. Second, MT3DMS results are compared with simulations by the finite element code FEFLOW version 5.3 (Diersch 2002, Table 1) and numerical results computed by the SEAWAT code version 4.0 (Langevin et al. 2008). The fore commercial software package has already been used in numerous studies for simulating heat transport of GSHP systems (e.g., Nam et al. 2008; Rühaak et al. 2008; Kupfersberger 2010).

MT3DMS is very attractive for heat transport modeling. It is probably the most popular finite difference code used for 3D simulation of multi-species solute transport in groundwater systems. A major advantage of using MT3DMS for heat transport simulation is that it integrates five different advection solver methods, which are suitable for solving problems in a broad range of hydrogeological and transport conditions. It also allows the user to flexibly enter crucial transport parameters such as diffusivity and dispersivity in form of arrays. Last but not least, as an open source code, it can be modified, extended, and adjusted to specific modeling requirements and individual application cases.

Implementation of the Model

Symbol	Variable	Unit
K_d	Distribution coefficient	(m^3/kg)
C^k	Dissolved mass concentration	(kg/m^3)
q_{ss}	Volumetric flow rate per unit volume of aquifer representing sources and sinks	(m^3/s/m^3)
q_h	Heat injection/extraction	(W/m^3)
C_{ss}	Concentration of the sources or sinks	(kg/m^3)
F_o	Energy extraction (point source)	(W)
F_L	Energy extraction per unit length of the borehole (line source)	(W/m)
F_A	Energy extraction per area of the source (planar source)	(W/m^2)
L	Characteristic length (grid spacing)	(m)
λ_m	Effective thermal conductivity of the porous media	(W/m/K)
λ_w	Water thermal conductivity	(W/m/K)
λ_s	Solid thermal conductivity	(W/m/K)
n	Porosity	(–)
ρ_w	Density of water	(kg/m^3)
c_w	Specific heat capacity of the water	(J/kg/K^1)
$\rho_w c_w$	Volumetric heat capacity of the water	(J/m^3/K^1)
ρ_s	Density of the solid material (=minerals)	(kg/m^3)
c_s	Specific heat capacity of the solid	(J/kg/K)
$\rho_s c_s$	Volumetric heat capacity of the solid	(J/m^3/K)
ρ_b	Dry bulk density $\rho_b = (1 - n)\rho_s$	(kg/m^3)
α, α_l	Dispersivity, longitudinal dispersivity	(m)
α_{th}	Transverse horizontal dispersivity	(m)
α_{tv}	Transverse vertical dispersivity	(m)
$q = v_f$	Darcy velocity	(m/s)
v_a	Seepage velocity	(m/s)
D_m, D_h	Molecular diffusion, thermal diffusivity	(m^2/s)
D_l	Longitudinal heat dispersion coefficient	(m^2/s)
D_{th}	Transverse horizontal heat dispersion coefficient	(m^2/s)
D_{tv}	Transverse vertical heat dispersion coefficient	(m^2/s)
x, y, z	Cartesian coordinates	(m)
R	Radial coordinate	(m)
Y	Dimension (length) of the source in y direction	(m)
Z	Dimension (length) of the source in z direction	(m)
ΔT	Temperature difference	(K)
ΔT_o	Temperature difference at the source	(K)
t	Time	(s)

Symbol	Variable	Unit
T, T_s	Temperature, temperature of the solid	(K)
T_u	Undisturbed temperature of the underground	(K)
R	Retardation factor	(–)
E_i	Exponential integral function	(–)
η	Integration parameter	(–)
K_o	Modified Bessel function of second kind and order zero	(–)

Governing Equations

Owing to the analogies between solute and heat transport processes, the governing equations for transport in the subsurface can be represented by similar differential equations. The partial differential equation for solute transport in transient groundwater flow systems solved by MT3DMS can be written as follows (Zheng and Wang 1999):

$$\left(1+\frac{\rho_b K_d}{n}\right)\frac{\partial C^k}{\partial t} = \mathrm{div}[(D_m+\alpha v_a)\mathrm{grad}C^k] - \mathrm{div}(v_a C^k)+\frac{q_{ss}C_{ss}}{n} \quad (1)$$

The left side represents the transient term multiplied by the retardation factor R. This dimensionless factor denotes the ratio between the total solute concentration and the mobile solute concentration given by the distribution of the contaminant in the fluid and solid phases.

The first term in the right side of Equation 1 is the hydrodynamic dispersion term, including pure molecular diffusion (D_m) and mechanical dispersion (αv_a). The second term describes advection and the third term represents source and sinks.

Analogously, the heat transport equation can be characterized by the principle of heat conservation, including conduction and convection (de Marsily 1986):

$$n\rho_w c_w\frac{\partial T}{\partial t}+(1-n)\rho_s c_s\frac{\partial T_s}{\partial t} = \mathrm{div}[(\lambda_m+n\rho_w c_w\alpha v_a)\mathrm{grad}T] - \mathrm{div}(n\rho_w c_w v_a T)+q_h \quad (2)$$

Assuming that the temperature of water and soil are the same, and that there is no net transfer from one phase to another, that is, thermal equilibrium (Nield and Bejan 2006), the term on the left side of the heat transport equation can be expressed as follows:

$$n\rho_w c_w\frac{\partial T}{\partial t}+(1-n)\rho_s c_s\frac{\partial T_s}{\partial t}=\rho_m c_m\frac{\partial T}{\partial t} \quad (3)$$

in which $\rho_m c_m$ denotes the volumetric heat capacity of the porous medium. It can be computed as the weighted arithmetic mean of solid rock and pore fluid (Anderson 2005; Hsu 2005; Hoehn and Cirpka 2006):

$$\rho_m c_m = n\rho_w c_w+(1-n)\rho_s c_s = n\rho_w c_w+\rho_b c_s \quad (4)$$

Using Equations 2 and 3, and rearranging them, Equation 2 simplifies to:

$$\left(\frac{\rho_m c_m}{n\rho_w c_w}\right)\frac{\partial T}{\partial t} = \mathrm{div}\left[\left(\frac{\lambda_m}{n\rho_w c_w}+\alpha v_a\right)\mathrm{grad}T\right] - \mathrm{div}(v_a T)+\frac{q_h}{n\rho_w c_w} \quad (5)$$

Conforming Coefficients

In order to relate Equations 1 and 5, the coefficients are compared as follows and each term and its implementation in MT3DMS are described in more detail:

- Retardation factor and distribution coefficient (thermal equilibrium)

The retardation factor (R) and the distribution coefficient (K_d) represented in the solute transport equation as solute sorption can be equivalently expressed in the heat transport equation as the heat exchange between the solid and the water. The retardation factor for heat is given as the ratio between volumetric heat capacity of the porous medium (total phase) and volumetric heat capacity of the water (mobile phase) (Shook 2001). The distribution coefficient is expressed as the ratio between the specific heat capacity of the solids and the volumetric heat capacity of the water:

$$R=\frac{\rho_m c_m}{n\rho_w c_w} \quad (6)$$

$$K_d=\frac{c_s}{\rho_w c_w} \quad (7)$$

(1) The new distribution coefficient for heat transport is implemented in MT3DMS in the *Chemical Reaction Package*. The type of sorption must be set to a *linear isotherm* (ISOTHM = 1) in order to keep the temperature exchange rate between the solid and the water constant independently of changes in temperature.

- Diffusion and dispersion coefficients

In the diffusion and dispersion term of the partial differential equation for solute transport (Equation 1), we identify two parts. The first one is the pure molecular diffusion term (D_m) that represents a process driven only by the concentration gradient. In the heat transport equation, it is equivalent to the thermal diffusivity driven by the temperature gradient:

$$D_h=\frac{\lambda_m}{n\rho_w c_w} \quad (8)$$

The second term of Equation 1, the hydrodynamic dispersion ($\alpha\ v_a$), is a process driven by the differences in flow velocities at pore scale. For the implementation in MT3DMS, the heat dispersivity coefficient is analogously applied as in solute transport (Anderson 2005).

(2) The new diffusion coefficient and the dispersivity coefficient are set in the *Dispersion Package*.

- Sources and sinks

The source and sink term in the solute transport equation represent the mass entering or leaving the domain. In the heat transport equation, this source and sink term indicate energy input or extraction.

$$q_{ss}C_{ss} = \frac{q_h}{\rho_w C_w} \tag{9}$$

To be consistent with the dimensions relating the contaminant and heat transport, the unit Kelvin (K) is equivalent to the concentration (kg/m^3). Thus energy input/extraction is stated similar as a mass load per unit volume of aquifer.

(3) The new source and sink term for heat transport is implemented in MT3DMS in the *Sink & Source Mixing Package*, and the type of source must be set to a *mass-loading source* (ITYPE0 = 15).

Limitations

Temperature has an influence on several physical parameters such as density and viscosity of water, and thermal conductivity and heat capacity of the porous medium (Figure 2). The principal limitation of the application of MT3DMS for heat transport simulation is that these relationships are not taken into account. Density and viscosity would directly affect the groundwater flow calculation and, consequently, affect the heat transport through the hydraulic conductivity. So the question is what role does this limitation play within the temperature spectrum typical for closed GSHP systems? Commonly, groundwater temperature changes are restricted by installation guidelines or occasionally by governmental environmental agencies (e.g., Hähnlein et al. 2008). For instance, in Switzerland, the maximum allowed temperature difference induced from geothermal energy use is 3 K (GSchV 2001). As a simple example, the physical relationship of hydraulic conductivity with density and viscosity is considered (Bear 1972). The behavior of hydraulic conductivity in regard to temperature is shown in Figure 2a, which shows an approximately linear trend in a range from 0 °C to 40 °C. Computation of the hydraulic conductivity for a usual temperature range disturbance of the groundwater under the presence of a GSHP system (from 7 °C to 10 °C, being 10 °C an approximation of the average annual temperature in Central Europe) yields an error of about 8%. Nevertheless, this inaccuracy seems acceptable in view of the imprecision related to the

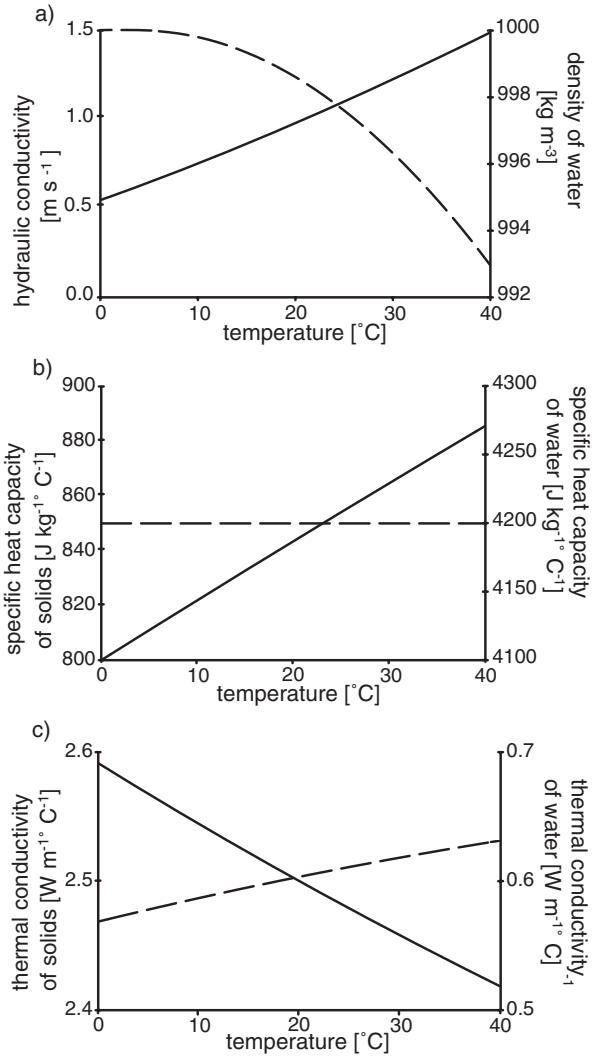

Figure 2. Thermal dependencies of: (a) hydraulic conductivity and density of the water, (b) thermal conductivity of solids and water, and (c) specific heat capacity of solids and water. Left axes are associated with the solid lines; right axes are associated with the dashed lines.

determination of hydraulic conductivity, which is already reported as 27% for laboratory conditions (Butters and Duchateau 2002).

Temperature variations can also promote free convection, which is a process driven by density differences as well as salinity concentration (Nield and Bejan 2006). Free convection creates a buoyancy effect, making a denser fluid flow below the lighter one. However, in the absence of brine currents in shallow aquifers, density changes are weak (Kolditz et al. 1998). Buoyancy effects begin to be important for density differences larger than 0.8 kg/m^3 (Schincariol and Schwartz 1990). Neglecting salinity effects, a density variation of 0.8 kg/m^{3}implies a temperature change from 0 °C to 15 °C. Aside from this, it should be noted that GSHP systems usually only operate some hours per day rather than continuously. Therefore, only temperature changes of few degrees are caused in the proximities of the BHE, which are shown to

be gradually balanced by the heat carried by the groundwater. For systems in which higher temperature changes are expected ($\gg$ 10 K), however, heat transport simulation with MODFLOW-MT3DMS should be done with the awareness that substantial errors due to neglected physical temperature dependencies are very likely to occur.

Figures 2b and 2c show the influence of temperature on heat capacity and thermal conductivity (Holzbecher 1998; Clauser 2003). Maximum differences in thermal conductivities and heat capacities for a usual temperature range disturbance of the groundwater under the presence of a GSHP system (from 7 °C to 10 °C) are less than 2%. As a simple example, simulations including thermal conductivity and heat capacity dependences on temperature are set up. The corresponding errors in the heat transport simulation are less than 0.5%. Even for larger differences (up to 60 °C), the error in the heat transport simulation is less than 3%. Based on these observations, the temperature dependency of the thermal parameters is not a real limitation for heat transport simulation of shallow geothermal systems.

Evaluation Procedure

The evaluation procedure is as follows: (1) MT3DMS numerical results are compared with analytical solutions for three scenarios (2D and 3D cases), and (2) for the same scenarios, MT3DMS results are compared with numerical results obtained by two alternative heat and contaminant transport numerical codes. A short description of the analytical solutions is given in Appendix. The finite element software FEFLOW (version 5.3) and the variable fluid density and viscosity code SEAWAT (version 4.0) are used for the second part of the evaluation.

Comparison Metric

Comparison of the simulations is based on residual errors and follows the method of efficiencies (EF) described by Loague and Green (1991):

$$\mathrm{EF} = \frac{\sum_{i=1}^{n} (X_{(i)} - \overline{X})^2 - \sum_{i=1}^{n} (X'_{(i)} - X_{(i)})^2}{\sum_{i=1}^{n} (X_{(i)} - \overline{X})^2} \qquad (10)$$

$X_{(i)}$ correspond to the results from the analytical solution or the alternative numerical codes (which we treat as observed or "true" values), $\overline{X}$ is the mean of the observed values, and $X'_{(i)}$ are the values simulated by MT3DMS. The maximum value for EF is 1, representing no difference between analytical and simulated results. The larger the residual error the closer the value of EF is 0. Computed EF values can even be negative; in this case the simulated values are assumed to be wrong. According to Green and Stephenson (1986), the advantage of the method of efficiencies is that it allows for a dimensionless estimation of goodness-of-fit in contrast to other methods based on dimensional data, such as root mean square error (RMSE) and mean deviation. A disadvantage of the method of efficiencies occurs when values involved vary over many orders of magnitude. However, it should work well for the moderate range of temperatures considered in this work. Efficiency values increase to unity as the agreement between simulated and observed values improves. For the sake of simplicity, we classify the efficiency results as the following: very good, for EF values between 0.98 and 1.00; good for EF ranging from 0.80 to 0.97; and moderate, for the range from 0.50 to 0.79. Below 0.50, the results are considered unsatisfactory.

The three scenarios are classified according to their respective Péclet number (Table 2). For instance, Domenico and Schwartz (1990) define the Péclet number for energy transport as:

$$\mathrm{Pe} = \frac{q l \rho_w C_w}{\lambda_m} \text{ with } \lambda_m = n\lambda_w + (1-n)\lambda_s \qquad (11)$$

The Péclet number relates the transport of energy by bulk fluid motion to the energy transport by conduction, that is, it is the ratio between heat convection and heat conduction. Scenarios 1 and 3 represent conduction and convection-dominated problems, respectively. In scenario 1, no groundwater flow is considered, compared with the relatively high flow velocity of scenario 3. Scenario 2 renders an intermediate case in which the convection and conduction processes have a similar influence (Pe = 1).

Model Setup

In this section, the model configurations used in the numerical codes (MODFLOW, MT3DMS, FEFLOW, and SEAWAT) are explained in detail. For the 2D scenarios, a one-layer rectangular domain representing a confined aquifer is simulated by the finite differences codes (Figure 3). The domain size is 300 m × 200 m with a basic regular grid spacing ($\Delta x = \Delta y = 0.5$ m). The BHE is represented by one source cell (positioned at $x = 50$ m, $y = 100$ m) of size 0.1 m × 0.1 m, where energy is extracted. For this, close to the source cell, the mesh is gradually refined from 0.5 m (regular grid spacing) to 0.1 m. Vertical heat transfer is ignored for the 2D cases, but included in the 3D simulations. The 3D simulations have 13 identical uniform 1-m layers. The BHE for the 3D scenarios is represented as point source by three cells within the three middle layers (sixth, seventh, and eighth layers) with the same coordinates as for the 2D case.

MODFLOW-2000 is used for steady-state flow field calculations when employing MT3DMS. In all three

Table 2
Scenarios Classified According to the Underlying Thermal Péclet Numbers (Pe)

Scenario	Pe	Gradient	Seepage Velocity (v_a) (m/s)
1	0	0	0
2	1	1.2×10^{-4}	3.7×10^{-6}
3	10	1.2×10^{-3}	3.7×10^{-5}

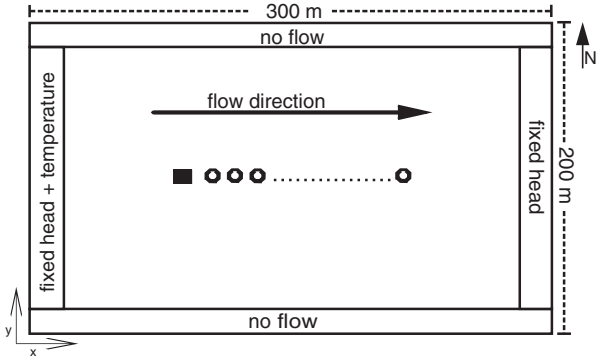

Figure 3. Model setup used for all scenarios with fixed head boundary conditions at west and east. Temperature boundary condition: fixed temperature at west border (285.15 K or 12 °C). Black square represents the BHE, circles denote the arrangement of observation points. For the 3D model, the source is located in layers 6, 7, and 8, and the observation points are located in the seventh layer.

scenarios, Dirichlet boundary conditions are assigned to the east and west boundaries of the flow model. For scenario 1, equal hydraulic head values are assigned resulting in no background flow. For scenarios 2 and 3, different head values are to produce a uniform flow gradient to the east. Hydraulic conductivity is homogenous and set to 8×10^{-3} m/s, which is within the range of typical sand aquifers (Spitz and Moreno 1996). An initial uniform density of 999.49 kg/m^3 is assumed for the whole domain.

An initial temperature of 285.15 K is assigned to the entire domain. Constant thermal boundary conditions (Dirichlet) are applied only at the west boundary. At the north and south boundaries, thermal flows are avoided to maintain a solution that can be compared with the analytical solution. At the BHE source cell, a continuous energy extraction of 60 W/m is set (Equation 9). This value is based on reference values from the German Engineer Association guidelines for thermal use of the underground (VDI-Richtlinie 4640 2001). Table 3 lists the thermal parameters entered in the numerical codes. Simulations are run until steady-state conditions are reached. Numerical results are saved at 200 observation points located east of the source cell. For the scenarios with groundwater flow, the monitoring points are located on the centerline of the plume. The third-order TVD (Total-Variation-Diminishing, ULTIMATE solver) scheme is used to solve for the advection term in all scenarios while the generalized conjugate gradient (GCG) solver is employed for the nonadvective terms. In order to fulfill the stability criteria related to the third-order TVD scheme, automatic time step estimation was selected.

Prior to the final mesh design described in the preceding sections, various domain and source cell sizes were examined for the convection-dominated case (scenario 3). This scenario is used due to the extensive spread of the temperature plume downgradient. Numerical simulations were compared with the analytical solution for a line source (Equation A3). The discrepancies are measured by model efficiencies and listed in Table 4. Figure 4 depicts the influence of different sized source cell on the simulated temperature. As expected, smaller source cells improve the agreement, since the referenced analytical model assumes an infinitely small source. This cannot be practically implemented in the numerical model, and thus a realistic size of 0.1 m × 0.1 m based on the size of a typical BHE is selected for further analysis.

The domain size of 300 m × 200 m is chosen to avoid boundary effects and because a larger area would extend computational time while only slightly reducing numerical error (Table 4). Similar arguments explain the choice to set 13 layers for the 3D case. For the 3D solution, vertical heat transfer across the boundaries may be of concern. No vertical heat flow is selected, to maintain consistency with the analytical solution. In very shallow systems, this may not be a valid approach.

Table 3
MT3DMS Specification for All Scenarios

Symbol	Variable	Value	Unit	MT3DMS Package
n	Porosity	0.26	(–)	BTN
λ_m	Effective thermal conductivity of the porous media	2.0	(W/m/K)	—
$\rho_w c_w$	Volumetric heat capacity of the water	$4.18 \times 10^{+6}$	(J/m^3/K)	—
ρ_s	Density of the solid material (= minerals)	2650	(kg/m^3)	—
c_s	Specific heat capacity of the solid	880	(J/kg/K)	—
ρ_b	Dry bulk density	1961	(kg/m^3)	RCT
K_d	Partition coefficient	2.10×10^{-4}	(m^3/kg)	RCT
α_l	Longitudinal dispersivity	0.5	(m)	DSP
α_{th}	Transverse horizontal dispersivity	0.05	(m)	DSP
α_{tv}	Transverse vertical dispersivity	0.05	(m)	DSP
D_h	Thermal diffusivity	1.86×10^{-6}	(m^2/s)	DSP
Tu	Undisturbed temperature of the ground	285.15	(K)	BTN
R	Retardation factor	2.59	(–)	RCT

Note: Last column indicates the name of the corresponding package within MT3DMS.

Table 4
Preparatory Phase: Model Efficiencies for Trial Runs with Different Mesh Sizes, Numbers of Layers, and Cell Sizes at the Source Cell

2D Case							
Model size (m × m)	100 × 100	200 × 200	300 × 300	400 × 400	500 × 500	700 × 700	1000 × 1000
Efficiency	−1.00	0.98	0.98	0.98	0.98	0.97	0.97
3D Case (using a 500 m × 500 m model size and 0.10 m × 0.10 m source cell size)							
Number of layers	3	5	7	9	11	13	15
Efficiency	0.52	0.83	0.87	0.88	0.89	0.89	0.89
Source Cell Size							
Cell size (m × m)	10 × 10	5 × 5	3 × 3	1 × 1	0.5 × 0.5	0.10 × 0.10	
Efficiency	−2.00	−0.91	−0.24	0.57	0.80	0.98	

Notes: For the 3D analyses, each model layer is 1 m thick. Efficiencies are for comparison between MT3DMS and the analytical results.

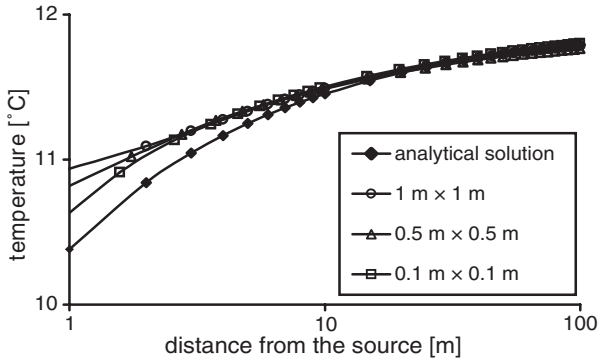

Figure 4. Comparison of 2D numerical and analytical solution (Equation A3) for three source cell sizes in the numerical solution. The values in the legend represent the local discretization Δx and Δy at and around the source cell.

Temperature gradients at shallow depths can be steep and dynamic, so that a substantial error may be introduced in the simulation by prohibiting heat flow at the top boundary. However, seasonal variability nearly diminishes below a depth of approximately 10 m (Anderson 2005). In addition, the relatively deep installation of typical GSHP systems of around 100 m or more with clearly dominating lateral heat gradients affirms the assumption to treat the BHE of such systems as a line source.

For the FEFLOW model setup, a triangular mesh (about 1 m element size) is chosen with the same type of boundary conditions and flow and thermal input parameters (Table 3). The source definition for the 2D cases is represented by a heat flux in one node. This introduces some inconsistency with MT3DMS, in which the energy extraction (expressed as mass loading) is applied to the cell volume (for 2D cases this volume is 0.01 m^3). For 3D cases, in FEFLOW, the source is also defined as heat flux in one node in three layers. In MT3DMS, the source is applied in three cells of total cell volume of 0.03 m^3. Consequently, although the realized energy extraction is the same (60 W/m) in both codes, the source definition in FEFLOW differs from MT3DMS, particularly for the 3D scenarios. In addition, FEFLOW, like SEAWAT, is fully coupled and consequently accounts for temperature dependencies of the flow and thermal parameters. The MT3DMS results lack this capability.

Since SEAWAT is based on the MODFLOW and MT3DMS codes, the model setup described previously for MT3DMS is used. The respective input parameters that account for the temperature dependencies of the fluid density and viscosity are included. The reference fluid density and viscosity are 999.49 kg/m^3 and 1.2×10^{-3} kg/m/s, respectively, corresponding to the initial ambient temperature of 12 °C. The equation after Pawlowski (1991) relating dynamic viscosity with temperature is used in the viscosity package (Langevin et al. 2008). Since the unique source in the model is a BHE, only temperature changes in the aquifer are expected to occur. Therefore, dependence of fluid density on concentration and pressure is not activated in the density input file within the SEAWAT code.

Results and Discussion

Comparisons with Analytical Solutions

Simulations of MT3DMS, by analytical methods, FEFLOW and SEAWAT, are compared using the method of efficiencies. Efficiencies are calculated for two sectors: the proximate sector encompasses the observation points near the source (from 1 to 10 m) and the distant sector, those from 10 to 100 m. For scenarios 2 and 3, which include convection, observation points are located downgradient of the heat source. Table 5 shows the efficiencies for each of the 2D and 3D scenarios. Results for each sector assuming steady-state or transient conditions (10 days) are also included.

First, MT3DMS simulations without groundwater flow (scenario 1) are compared with the corresponding

Table 5
Efficiencies of the Comparison Between MT3DMS and Analytical Results, Steady-State and Transient Conditions

	2D				3D			
	<10 m		>10 m		<10 m		>10 m	
Scenario	Steady State	Transient	Steady State	Transient	Steady State	Transient	Steady State	Transient
1 (no flow)	—	0.98	—	1.00	—	—	—	—
2 (Pe = 1)	0.99	1.00	0.99	1.00	0.93	0.96	1.00	1.00
3 (Pe = 2)	0.96	0.96	0.96	1.00	0.92	0.84	0.94	1.00

Note: Two sectors are distinguished: proximate, from 1 to 10 m distance (downgradient) from the source; and distant, from 10 to 100 m.

analytical results based on line source theory (Equation A1). For the analytical solution, as time tends to infinity, the heat plume extends infinitely (e.g., Diao et al. 2004), that is, no steady condition is reached. Therefore, results are compared only for transient conditions over a period of 10 days (Figure 5a). The calculated efficiency is 0.98 for the first sector, while for larger distances it reaches a value of 1.0, representing a very good agreement between both curves (Table 5). The deviation close to the source is mostly due to the limitation of representing an infinitesimal line source numerically. Numerical results from scenarios 2 and 3 (moderate case [Pe = 1] and convection-dominated scenario [Pe = 10]) are compared with analytical solutions presented by Metzger et al. (2004, Equation A2) and Diao et al. (2004, Equation A3); steady-state and transient results are shown in Figures 5b and 5c. The computed efficiencies are listed in Table 5. The transient curves (results for 10 days) illustrate a steep temperature gradient for about 2 m from the source for scenario 2 and 15 m for scenario 3; at greater distances, the curves become constant to the ambient temperature (12 °C). This trend clearly indicates that these transient temperature disturbances remain fairly close to the source. For steady-state conditions, however, the thermal change extends beyond the furthest observation point (located at 100 m approximately). This pattern is observed in both scenarios (Pe = 1 and 10); a similar behavior is also observed in the 3D cases discussed in the next paragraph. Scenario 2 shows a very good agreement between analytical and numerical results. High efficiencies for steady-state and transient conditions are obtained. Once again, discrepancies between results close to the source (first two to three observation points) are due to the cell-based representation of the source by the numerical method. A good fit is also obtained for scenario 3; however, the efficiencies in the sectors for steady-state conditions are somewhat lower, 0.96. This slight decrease in efficiency may reflect some numerical dispersion when applying the third-order TVD solver for such convection-dominated conditions.

Of interest are also the absolute temperature differences (ΔT) under steady state conditions. For scenario 2,

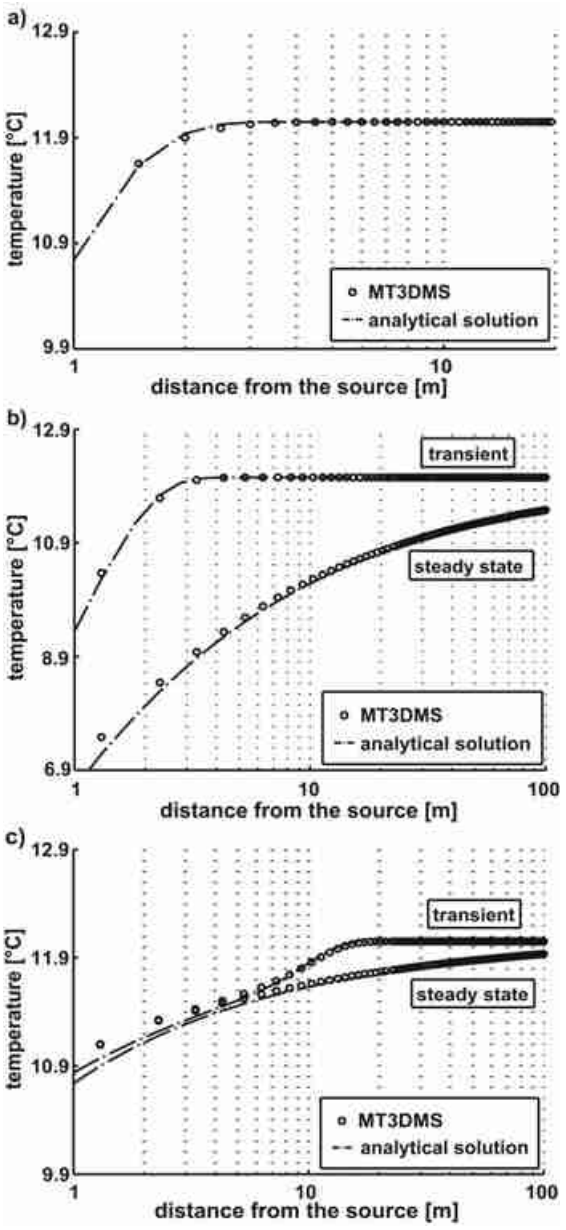

Figure 5. Numerical and analytical results for the 2D cases. (a) Scenario 1 (no flow), (b) scenario 2 (Pe = 1), and (c) scenario 3 (Pe = 10). Transient results are shown for 10 days.

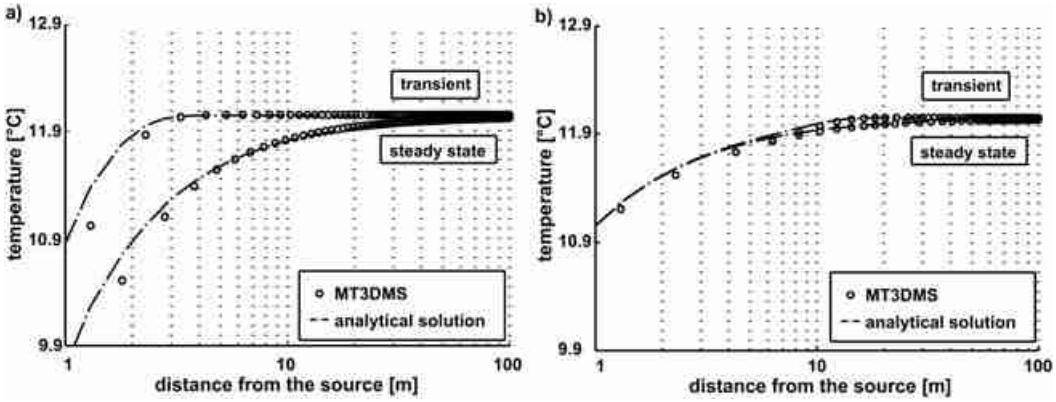

Figure 6. Numerical and analytical results for the 3D cases. (a) Scenario 2 (Pe = 1) and (b) scenario 3 (Pe = 10). Transient results are shown for 10 days.

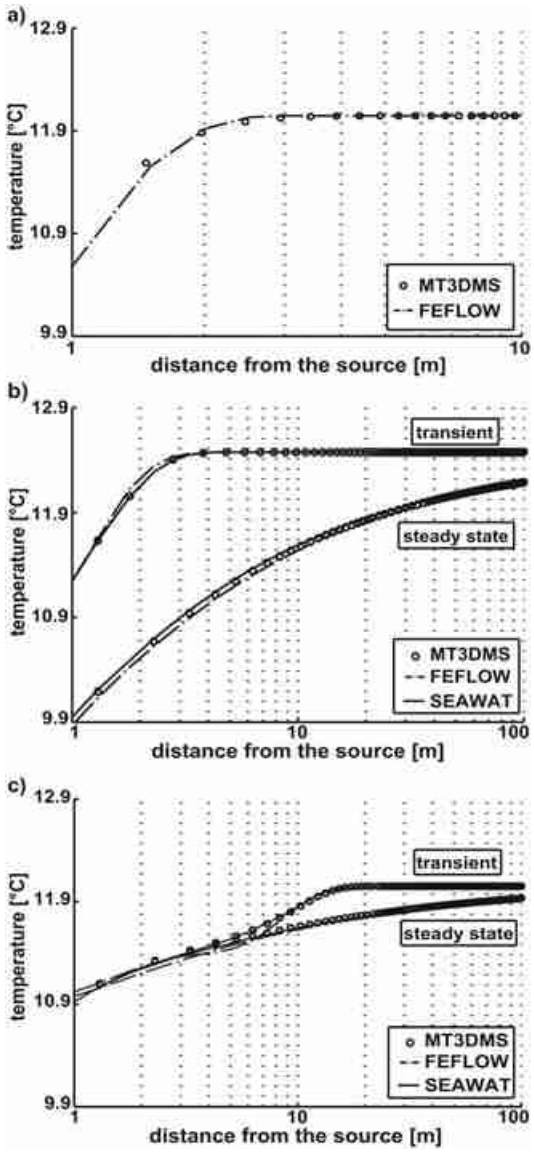

Figure 7. Comparison of MT3DMS, FEFLOW, and SEAWAT results for the 2D cases. (a) Scenario 1 (no flow), (b) scenario 2 (Pe = 1), and (c) scenario 3 (Pe = 10). Transient results are shown for 10 days.

a $\Delta T = 5$ K is computed 1 m downgradient from the source, and $\Delta T = 1$ K for scenario 3. Apparently, the convection-dominated regime brings out a lower absolute temperature change close to the source. This reflects the important role of groundwater flow for the energy supply at the borehole.

For the 3D cases, numerical results are compared with an analytical solution with a planar source for heat transport based on classical solute transport equations (Domenico and Robbins 1985; Equation A5). Scenario 1 (no flow; Pe = 0) is not considered due to the lack of a 3D analytical solution for pure conduction. The calculated efficiencies are shown in Table 5. Figure 6a shows good to very good agreement between steady-state and transient numerical and analytical results for scenario 2 (Pe = 1) at the proximate sector and the distant sector, respectively. Overall, the discrepancies for scenario 3 (Pe = 10) are small for both steady-state and transient (Figure 6b). As for 2D scenario 3, the fit is slightly worse (efficiencies are smaller) close to the source. Again, this is caused by the difference in how the source is represented in the two solutions. The 3D analytical solutions A4 and A5 consider a semi-infinite medium and therefore they neglect upgradient spreading. Accordingly, for consistency, thermal conductivity and dispersivity are set to zero in the area upgradient from the source in MT3DMS. Nevertheless, a semi-infinite medium and a planar source cannot be exactly represented in the numerical code. The absolute temperature differences at 1 m distance from the source for the 3D case are the same as for 2D cases, being $\Delta T = 4$ K and $\Delta T = 1$ K.

Comparisons with Numerical Solutions

Figures 7 and 8 show results from SEAWAT, MT3DMS, and FEFLOW for 2D and 3D, respectively. The computed efficiencies for MT3DMS and SEAWAT results are presented in Table 6. The close match between MT3DMS and SEAWAT is consistent with the overall efficiency of 1.0 for all cases. Comparison with FEFLOW shows that for 2D there is good to very good agreement, and model efficiencies range between 0.91 and 1.0. Efficiencies are always lower close to the source

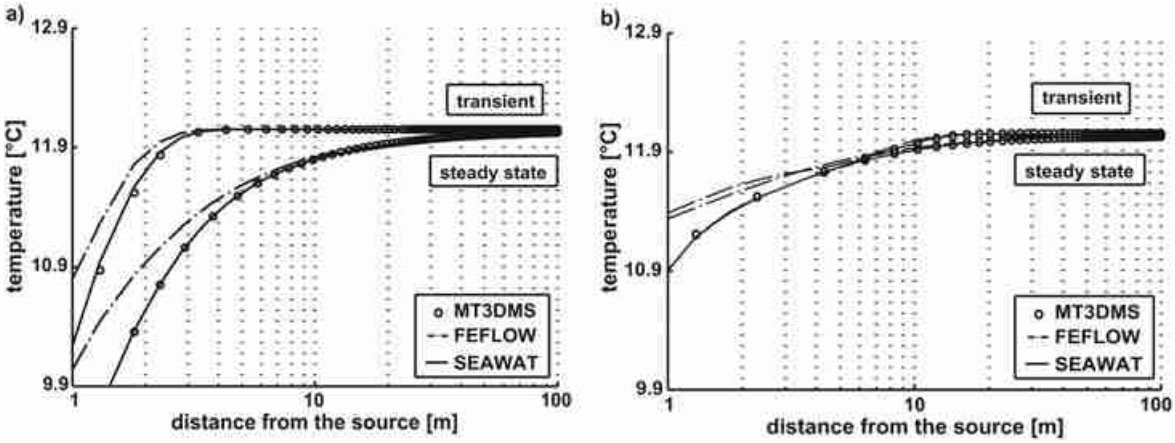

Figure 8. Comparison of MT3DMS, SEAWAT, and FEFLOW results for the 3D cases. (a) Scenario 2 (Pe = 1) and (b) scenario 3 (Pe = 10). Transient results are shown for 10 days.

Table 6
Model Efficiencies of the Comparison Between MT3DMS-SEAWAT and MT3DMS-FEFLOW Results

	2D				3D			
	<10 m		>10 m		<10 m		>10 m	
Scenario	Steady State	Transient	Steady State	Transient	Steady State	Transient	Steady State	Transient
SEAWAT								
1 (no flow)	—	—	—	—	—	—	—	—
2 (Pe = 1)	1.00	1.00	1.00	1.00	1.00	1.00	1.00	1.00
3 (Pe = 10)	1.00	1.00	1.00	1.00	1.00	1.00	1.00	1.00
FEFLOW								
1 (no flow)	—	—	—	—	—	—	—	—
2 (Pe = 1)	0.99	0.99	1.00	1.00	0.64	0.64	0.93	1.00
3 (Pe = 10)	0.93	0.91	0.95	0.97	0.64	0.64	0.87	1.00

Note: Two sectors are distinguished: proximate, from 1 to 10 m distance (downgradient) from the source; and distant, from 10 to 100 m.

and are a little lower away from the source for case 3 (Pe = 10). These differences are likely to be dominated by differences in how the source is represented in MT3DMS and FEFLOW.

The very good agreement between the MT3DMS solution and SEAWAT suggests that the influence of fluid density and viscosity changes is minor within the temperature ranges in which GSHP systems usually operate. To further analyze the effect of the temperature dependence of the fluid parameters, scenario 1 (Pe = 1), which has the greatest range of temperatures, is additionally tested in FEFLOW with and without the temperature dependency option. Results from these simulations (data not shown) display an insignificant difference near the source between both temperature profiles. A minor change in the efficiency value (<0.01) is computed. This result again demonstrates that temperature dependencies barely influence simulation of the GSHP systems for the specified conditions.

For the 3D scenarios (Figure 8), moderate efficiencies are obtained close to the source. This may be attributed to the different source definition. In MT3DMS, the energy is extracted from a cell volume, whereas in the FEFLOW code the energy extraction is assigned to a node. The latter is more similar to a line source than the planar source used in the analytical solution. Therefore, the MT3DMS-based results are closer to the analytical solution. However, the difference in these scenarios may also be affected by different influences of numerical dispersion. The latter is minimized by the transport solution technique used in MT3DMS (TVD method). In FEFLOW, the standard Galerkin method (GFEM) is used, which possibly causes more numerical dispersion in the results. For transient conditions, the match between the numerical curves and hence the efficiencies is much better in both sectors.

Of particular interest are the execution times (computational times necessary to perform a single simulation) of the two finite difference codes. MT3DMS and SEAWAT simulations are performed using the same model setup and solution techniques (with same convergence criterion). Table 7 presents run times for scenarios 2 and 3 given in seconds (2D and 3D). Execution times for scenario 1 are not shown since no significant differences are noticeable. Note that the period lengths used for scenarios 2 and 3

Table 7
Execution Time for the Different Scenarios

	Execution Time (s)			
	2D		3D	
Code	Scenario 2 (Pe = 1)	Scenario 3 (Pe = 10)	Scenario 2 (Pe = 1)	Scenario 3 (Pe = 10)
MT3DMS	238	1,070	5,484	20,051
SEAWAT	507	1,595	11,114	31,737

Hardware specifications: Pentium IV, CPU 3 GHz, and 1 GB RAM.

are 2000 and 800 days, respectively. In general, SEAWAT requires longer running times for the same simulated scenarios than MT3DMS. For scenario 2 (2D and 3D), SEAWAT yields execution times that are approximately two times longer than MT3DMS. For scenario 3 (2D and 3D), SEAWAT running times are around 1.5 times longer than MT3DMS. Owing to significant differences between the simulation specifications in FEFLOW and those used in the finite differences codes, a comparison with the execution time of the finite element code is not meaningful. However, it should be pointed out that the computational effort with the model setup in FEFLOW was lower, resulting in shorter execution times for all simulations. For instance, execution times for scenario 2 are 162 and 645 s for 2D and 3D cases, respectively. This is likely attributed to a lower number of defined nodes, the type of solution techniques for the flow and the transport model and the time step calculation.

Conclusions

This work demonstrates the applicability of MT3DMS for heat transport of GSHP systems in a confined aquifer. Although originally developed for solutes, it can be reliably applied for simulation of heat transport in saturated porous media under the influence of closed GSHP systems that result in temperature variations similar to those considered in this work. We used three different single borehole scenarios for comparison, which differ with respect to the assumed groundwater flow velocities. The overall agreement of MT3DMS with analytical solutions, the SEAWAT code and the finite element model FEFLOW is good to very good. Differences are mostly due to the impossibility of representing the source characteristics (line source and planar source) of the analytical solutions in a numerical model, and the different ways MT3DMS and the commercial code FEFLOW allow the heat pump well to be represented. Model efficiencies for the pure conduction scenario and the moderate convection scenario are slightly more similar than for the convection-dominated scenario. This is interpreted as an effect of the numerical dispersion for high groundwater velocities. Moreover, the different source representations might also result in a discrepancy propagation downgradient.

For these realistic scenarios, highest absolute temperature differences 1 m from the source reach 5 K if heat is only transported by conduction and 1 K if convection dominates. MT3DMS does not account for the effects of temperature on density or viscosity. However, for the temperature ranges considered, the influence of the temperature dependencies appear not to be a limitation for simulation of closed loop systems. These findings are corroborated by: (1) the satisfactory agreement with FEFLOW results (fully coupled simulations) even though the two codes differ with respect to definition of the heat source and the transport solution techniques used and (2) the very good agreement between MT3DMS and SEAWAT (with efficiencies of 1.0 for all scenarios) even though fluid density and viscosity temperature dependencies are represented by SEAWAT. Considering that SEAWAT needs more execution time and the weak effect of the temperature changes on the hydraulic and thermal parameters, the use of MT3DMS is adequate providing the temperature changes exerted by the GSHP system are low (<5 K). An additional simulation using the moderate seepage velocity case (Pe = 1) and an increased energy extraction of 100 W/m (temperature change = 10 K) also shows a very good agreement between MT3DMS and SEAWAT (overall EF of 0.99) and a good agreement between MT3DMS and FEFLOW (EF of 0.94 and 0.98 for proximate and distant sectors, respectively).

It is recommended to take advantage of the accurate solutions and fast execution times of MT3DMS, but to test the constant-density assumption by running the same model with another code, for example, FEFLOW or SEAWAT. For open geothermal systems such as GWHPs and ATES systems, which might induce higher temperature differences in the aquifer, it may be necessary to use fluid density and viscosity variable codes such as SEAWAT or FEFLOW.

Application of MT3DMS for other shallow geothermal technologies such as open GWHP systems or ATES is an attractive prospect for future work. In addition, testing of the code in field cases is suggested to further explore the potential application range of MT3DMS for geothermal simulations.

Acknowledgments

The financial support for J. H.-M. and N. M.-G. from the Federal Ministry for Education and Research

(BMBF) scholarship program for International Postgraduate Studies in Water Technologies (IPSWaT) is profoundly acknowledged. This work was also supported by the GWAT-LCA project within the seventh framework program (Contract No. PIEF-GA-2008-220620). Furthermore, we would like to thank Prof. Dr. Peter Grathwohl for his suggestions and valuable support. The assistance of Margaret Hass in preparing the manuscript is also gratefully acknowledged. Last but not least, we would like to thank Dr. Chris Langevin, Prof. Dr. Chunmiao Zheng, Dr. Grant Ferguson, and Dr. Mary C. Hill for their pertinent and constructive comments and suggestions in reviewing the manuscript.

Appendix

Two-Dimensional Analytical Solutions

- Transient conditions, closed system, and no groundwater flow velocity. It applies for the response of an infinite and constant line source in a homogeneous, isotropic, infinite medium (Carslaw and Jäger 1959).

$$\Delta T(r,t) = \frac{F_L}{4\pi\lambda_m} E_i\left[-\frac{r^2}{4(\lambda_m/\rho_m C_m)t}\right] \quad \text{(A1)}$$

- Transient conditions, closed system, and groundwater flow velocity considering heat dispersivity. It applies for the response of an infinite and constant line source in a homogeneous, isotropic, infinite medium (Metzger et al. 2004).

$$\Delta T(x,t) = \frac{F_L}{4\pi n\rho_w c_w\sqrt{D_l D_{th}}} \exp\left[\frac{v_a x}{2D_l}\right] \int \frac{1}{\eta} \times \exp\left[-\eta - \frac{v_a^2 x^2}{16 D_{th}^2 \eta}\right] d\eta \quad \text{(A2)}$$

  where $D = \lambda_m/n\rho_w c_w + \alpha v_a$ is the heat dispersion coefficient (for longitudinal or transverse components).
- Steady-state conditions, closed system, and groundwater flow velocity (Diao et al. 2004). In order to consider heat dispersivity, the equation was modified. It applies for the response of an infinite and constant line source in a homogeneous, isotropic, infinite medium.

$$\Delta T(x) = \frac{F_L}{2\pi n\rho_w c_w D_{th}} \exp\left[\frac{v_a x}{2D_{th}}\right] K_0\left[\frac{v_a x}{2D_{th}}\right] \quad \text{(A3)}$$

Three-Dimensional Analytical Equation

- Transient and steady-state conditions, closed system, and groundwater flow velocity (Hähnlein et al. in press) based on solute transport analytical solutions (Fried et al. 1979; Domenico and Robbins 1985).

$$\Delta T(x,y) = \frac{F_o}{v_a n\rho_w c_w\sqrt{4\pi D_{th}(x/v_a)}} \times \exp\left(\frac{-v_a(y^2)}{4D_{th}x}\right) \quad \text{(A4)}$$

$$\Delta T(x,t) = \left(\frac{\Delta T_0}{2}\right) \operatorname{erfc}\left[\frac{(Rx - v_a t)}{2\sqrt{D_l R t}}\right] \times \operatorname{erf}\left[\frac{Y}{4(D_{th}(x/v_a))^{0.5}}\right] \times \operatorname{erf}\left[\frac{Z}{4(D_{tv}(x/v_a))^{0.5}}\right] \quad \text{(A5)}$$

References

Anderson, M.P. 2005. Heat as a ground water tracer. *Ground Water* 43, no. 6: 951–968.

Bächler, D. 2003. Coupled thermal-hydraulic-chemical modelling at the Soultz-sous-Forêts HDR Reservoir (France). Ph.D. diss., Swiss Federal Institute of Technology, Zurich.

Bear, J. 1972. *Dynamics of Fluids in Porous Media*. New York: American Elsevier Publishing Company Inc.

Bertani, R. 2005. World geothermal generation 2001–2005: State of the art. In *Conference Proceedings: World Geothermal Congress*, ed. R.N. Horne and E. Okandan. Reykjavik: Paper 0008.

Bethke, C., M.-K. Lee, and J. Park. 2007. *Basin Modeling with Basin2, Release 5.0.1*. Urbana Champaign, Illinois: Hydrogeology Program, University of Illinois.

Blum, P., G. Campillo, W. Münch, and T. Kölbel. 2010. CO_2 savings of ground source heat pump systems—a regional analysis. *Renewable Energy* 35, no. 1: 122–127.

Brehm, D. 1989. *Development, Validation and Application of a 3-Dimensional, Coupled Flow and Transport Finite Differences Model*. Giessen: Lenz Verlag.

Butters, G.L., and P. Duchateau. 2002. Continuous flow method for rapid measurement of soil hydraulic properties: I. Experimental considerations. *Vadose Zone Journal* 1, 239–251.

Carslaw, H.S., and J.C. Jäger. 1959. *Conduction of Heat in Solids*, 2nd ed. New York: Oxford University Press.

Cathomen, N. 2002. Wärmetransport im Grundwasser—Auswirkung von Wärmepumpenanlagen auf die Grundwassertemperatur am Beispiel der Gemeinde Altach im Vorarlberger Rheintal, Diploma Thesis, ETH Zürich, Switzerland.

Cathomen, N., F. Stauffer, W. Kinzelbach, and F. Osterkorn. 2002. Thermische Grundwassernutzung. Auswirkung von Wärmepumpenanlagen auf die Grundwassertemperatur. *Gas Wasser Abwasser* 82, no. 12: 901–906.

Chiasson, A.D., S.J. Rees, and J.D. Spitler. 2000. A preliminary assessment of the effects of ground water flow on closed-loop ground-source heat pump systems. *ASHRAE Transactions* 106, no. 1: 380–393.

Clauser, C. 2003. *Numerical Simulation of Reactive Flow in Hot Aquifers, SHEMAT and Processing SHEMAT*. Berlin: Springer Verlag.

Clauser, C. 2006. Geothermal energy. In *Landolt-Börnstein—Numerical Data and Functional Relationships*, ed. K. Heinloth, new series, vol. 8: *Energy Technologies, Subvolume 3: Renewable Energies*. Berlin: Springer Verlag.

de Marsily, G. 1986. *Quantitative Hydrogeology*. Orlando: Academic Press.

Diao, N., Q. Li, and Z. Fang. 2004. Heat transfer in ground heat exchangers with groundwater advection. *International Journal of Thermal Sciences* 43, no. 12: 1203–1211.

Diersch, H.J.G. 2002. *FEFLOW 5- User's Manual*. Berlin: WASY GmbH.

Domenico, P.A., and F.W. Schwartz. 1990. *Physical and Chemical Hydrogeology*, 2nd ed. New York: John Wiley & Sons Inc.

Domenico, P.A., and G.A. Robbins. 1985. A new method of contaminant plume analysis. *Ground Water* 23, no. 4: 476–485.

Eskilson, P. 1987. Thermal analysis of heat extraction boreholes. Ph.D. diss., Department of Mathematical Physics, Lund Institute of Technology.

Fan, R., Y. Jiang, Y. Yao, and Z. Ma. 2007. Theoretical study on the performance of an integrated ground-source heat pump system in a whole year. *Energy* 32, no. 11: 2199–2209.

Ferguson, G. 2009. Unfinished business in geothermal energy. *Ground Water* 47, no. 2: 167–167.

Florides, G., and S. Kalogirou. 2007. Ground heat exchangers—A review of systems, models and applications. *Renewable Energy* 32, no. 15: 2461–2478.

Fried, J.J., P. Muntzer, and L. Zilliox. 1979. Ground-water pollution by transfer of oil hydrocarbons. *Ground Water* 17, no. 6: 586–594.

Green I.R.A., and D. Stephenson. 1986. Criteria for comparison of single events models. *Hydrological Sciences Journal* 31, no. 3: 391–411.

GSchV. 2001. *Gewässerschutzverordnung*. Switzerland: GSchV.

Guimera, J., F. Ortuño, E. Ruiz, A. Delos, and A. Pérez-paricio. 2007. Influence of ground-source heat pumps on groundwater. In *Conference Proceedings: European Geothermal Congress*, Unterhaching.

Harbaugh, A.W., E.R. Banta, M.C. Hill, and M.G. Mcdonald. 2000. MODFLOW-2000, the U.S. Geological Survey modular ground water model, user guide to modularization concepts and the ground water flow process. USGS Open-File Report 00-92.

Hähnlein, S., N. Molina-Giraldo, P. Blum, P. Bayer, and P. Grathwohl. Ausbreitung von Kältefahnen im Grundwasser bei Erdwärmesonden (Cold plumes in groundwater for ground source heat pump systems). *Grundwasser*. In press.

Hähnlein, S., P. Grathwohl, P. Bayer, and P. Blum. 2008. Cold plumes of ground source heat pumps: Their length and legal situation. *Geophysical Research Abstracts 10*, EGU2008-A-07946.

Healy, R.W., and A.D. Ronan. 1996. Documentation of computer program VS2DH for simulation of energy transport in variably saturated porous media. USGS Water Resources Investigations Report 96-4230.

Hellström, G., and T. Schmidt. 2005. Ground source cooling—Working paper on usable tools and methods. EU Commission SAVE Programme and Nordic Energy Research.

Hoehn, E., and O.A. Cirpka. 2006. Assessing hyporheic zone dynamics in two alluvial flood plains of the Southern Alps using water temperature and tracers. *Hydrology Earth System Sciences* 10, no. 4: 553–563.

Holzbecher, E. 1998. *Modelling Density-Driven Flow in Porous Media*. New York: Springer Verlag.

Holzbecher, E., and C. Kohfahl. 2008. *Geothermics Modelling using COMSOL Multiphysics*. Seminar manual. Berlin.

Hsu, C.T. 2005. Dynamic modeling of convective heat transfer in porous media. In *Hand Book of Porous Media*, ed. K. Vafai, 2nd ed. Boca Raton: CRC-Taylor & Francis Group.

Kangas, M.T. 1996. Modeling of transport processes in porous media for energy applications. Ph.D. diss., Helsinki University of Technology.

Kipp, K.L. 1986. HST3D—A computer code for simulation of heat and solute transport in 3D ground water flow systems. USGS Water Resources Investigations Report 86-4095.

Kipp, K.L. Jr., P.A. Hsieh, and S.R. Charlton. 2008. Guide to the revised ground-water flow and heat transport simulator: HYDROTHERM—Version 3: U.S. Geological Survey Techniques and Methods 6-A25, 160 p.

Kohl, T., and R.J. Hopkirk. 1995. "FRACTure"—A simulation code for forced fluid flow and transport in fractured, porous rock. *Geothermics* 24, no. 3: 333–343.

Kolditz, O., A. Habbar, R. Kaiser, T. Rother, C. Thorenz, M. Kohlmeier, and S. Moenickes. 2001. ROCKFLOW user's manual release 3.5. Institute of fluid mechanics and computer applications in civil engineering. University of Hannover.

Kolditz, O., R. Ratke, H.J.G. Diersch, and W. Zielke. 1998. Coupled groundwater flow and transport: 1. Verification of variable density flow and transport models. *Advances in Water Resources* 21, no. 1: 27–46.

Kollet, S.J., I. Cvijanovic, D. Schüttemeyer, R.M. Maxwell, A.F. Moene, and P. Bayer. 2009. The influence of rain sensible heat and subsurface energy transport on the energy balance at the land surface. *Vadose Zone Journal* 8, no. 4: 846–857.

Kupfersberger, H. Application of groundwater heat transfer modeling to a regional aquifer in Austria. *Environmental Geology*. In press.

Langevin, C.D., D.T. Thorne Jr., A.M. Dausman, M.C. Sukop, and W. Guo. 2008. *SEAWAT Version 4: A Computer Program for Simulation of Multi-Species Solute and Heat Transport. U.S. Geological Survey Techniques and Methods. Book 6*, Chap. A22. Reston, Virginia: USGS.

Langevin, C.D., W.B. Shoemaker, and W. Guo 2003. MODFLOW-2000, the U.S. Geological Survey modular ground-water model-Documentation of the SEAWAT-2000 version with the variable-density flow process (VDF) and the integrated MT3DMS transport process (IMT). USGS Open-File Report 03-426.

Loague, K., and R.E. Green. 1991. Statistical and graphical methods for evaluating solute transport models: Overview and application. *Journal of Contaminant Hydrology* 7, no. 1–2: 51–73.

Lund, J.W., D.H. Freeston, and T.L. Boyd. 2005. Direct application of geothermal energy: 2005 worldwide review. *Geothermics* 34, no. 3: 691–727.

Martin, R.J., S.F. Bender, S.W. Gaulke, and J. Wallace. 2001. Simulation of groundwater flow and heat transport on Grand Cayman Island. In *MODFLOW 2001 and Other Modeling Odysseys, Conference Proceedings*, eds. S. Seo, E.P. Poeter, C. Zheng, O. Poeter, 776–782. International Ground Water Modeling Center, Colorado School of Mines, Golden, Colorado.

Medina, A., G. Galarza, and J. Carrera. 1996. TRANSIN III: Fortran code for solving the coupled non-linear flow and transport inverse problem. ETSE CCPB. UPC. El Berrocal Project. Topical Report 17. ENRESA.

Metzger, T., S. Didierjean, and D. Maillet. 2004. Optimal experimental estimation of thermal dispersion coefficients in porous media. *International Journal of Heat and Mass Transfer* 47, no. 14–16: 3341–3353.

Molson, J.W., and E.O. Frind. 2002. HEATFLOW, version 2.0 user guide. Department of Earth Sciences, University of Waterloo.

Nam, Y., R. Ookaa, and S. Hwanga. 2008. Development of a numerical model to predict heat exchange rates for a ground-source heat pump system. *Energy and Buildings* 40, no. 12: 2133–2140.

Nield, D.A., and A. Bejan. 2006. *Convection in Porous Media*, 3rd ed. New York: Springer.

Pawlowski, J. 1991. *Veranderliche Stoffgroben in der Ahnlichkeitstheorie*. Frankfurt: salle+sauerlander.

Pruess, K., C. Oldenburg, and G. Moridis. 1996. THOUGH2 User's Guide, version 2.0, Lawrence Berkeley National Laboratory Report LBL-38383, SN027.

Rühaak, W., P. Schätzl, A. Renz, and H.J.G. Diersch. 2008. Numerical modeling of geothermal processes: Issues and examples. 10th International Mine Water Association Congress, Mine Water and the Environment, Karlovy Vary.

Schincariol, R.A., and F.W. Schwartz. 1990. An experimental investigation of variable-density flow and mixing in homogeneous and heterogeneous media. *Water Resources Research* 26, no. 10: 2317–2329.

Schmidt, T., and G. Hellström. 2005. Ground source cooling—working paper on usable tools and methods. EU Commission SAVE Programme and Nordic Energy Research.

Shook, M.G. 2001. Predicting thermal breakthrough in heterogeneous media from tracer tests. *Geothermics* 30, no. 6: 573–589.

Šimùnek, J., M. Šejna, and Th. van Genuchten. 1999. The HYDRUS-2D software package for simulating the two-dimensional movement of water, heat, and multiples solutes in variable-saturated media, version 2. U.S. Department of Agriculture, Riverside.

Spitz, K., and J. Moreno. 1996. *A Practical Guide to Groundwater and Solute Transport Modeling*. New York: John Wiley & Sons Inc.

Therrien, R., R.G. Mclaren, E.A. Sudicky, and S.M. Panday. 2006. HydroGeoSphere: A three-dimensional numerical model describing fully-integrated subsurface and surface flow and solute transport, Groundwater Simulations Group, University of Waterloo.

Thorne, D., C.D. Langevin, and M.C. Sukop. 2006. Addition of simultaneous heat and solute transport and variable fluid viscosity to SEAWAT. *Computer and Geosciences* 32, no. 10: 1758–1768.

Tsang, C.F., T. Buscheck, and C. Doughty. 1981. Aquifer thermal energy storage: A numerical simulation of Auburn university field experiments. *Water Resources Research* 17, no. 3: 647–658.

VDI-Richtlinie 4640. 2001. *Thermische Nutzung des Untergrundes, teil 2. Verein Deutscher Ingenieure*. Düsseldorf: VDI-Verlag.

Voss, C.I., and A.M. Provost. 2002. SUTRA, a variable-density ground-water flow with solute or energy transport. USGS Water Resources Investigations Report 02-4231.

Zheng, C., and P.P. Wang. 1999. MT3DMS: A modular threedimensional multi-species transport model for simulation of advection, dispersion and chemical reactions of contaminants in groundwater systems; Documentation and user's guide. U.S. Army Engineer Research and Development Center Contract Report SERDP-99-1, Vicksburg, Mississippi, 202. http://hydro.geo.ua.edu/mt3d/.